The Astrophysical Journal, 744:178 (9pp), 2012 January 10 doi:10.1088/0004-637X/744/2/178


# CONSTRAINING DUST AND MOLECULAR GAS PROPERTIES IN Lyα BLOBS AT $z \sim 3$

Yujin Yang[1], Roberto Decarli[1], Helmut Dannerbauer[2,3], Fabian Walter[1], Axel Weiss[4], Christian Leipski[1], Arjun Dey[5], Scott C. Chapman[6], Emeric Le Floc'h[2], Moire K. M. Prescott[7,14], Roberto Neri[8], Colin Borys[9], Yuichi Matsuda[10], Toru Yamada[11], Tomoki Hayashino[12], Christian Tapken[13], and Karl M. Menten[4]
[1] Max-Planck-Institut für Astronomie, Königstuhl 17, Heidelberg, Germany
[2] Laboratoire AIM, CEA/DSM-CNRS-Université Paris Diderot, Irfu/Service d'Astrophysique, CEA-Saclay, Orme des Merisiers, 91191 Gif-sur-Yvette Cedex, France
[3] Universität Wien, Institut für Astronomie, Türkenschanz-strasse 17, 1180 Wien, Austria
[4] Max-Planck-Insitut für Radioastronomie, Auf dem Hügel 69, D-53121 Bonn, Germany
[5] National Optical Astronomy Observatory, 950 North Cherry Avenue, Tucson, AZ 85719, USA
[6] Institute of Astronomy, University of Cambridge, Madingley Road, Cambridge CB3 0HA, UK
[7] Department of Physics, Broida Hall, Mail Code 9530, University of California, Santa Barbara, CA 93106, USA
[8] IRAM-Institut de Radio Astronomie Millimétrique, 300 rue de la Piscine, 38406 Saint-Martin d'Hères, France
[9] IPAC, California Institute of Technology, 1200 East California Boulevard, Pasadena, CA 91125, USA
[10] Department of Physics, Durham University, South Road, Durham DH1 3LE, UK
[11] Astronomical Institute, Tohoku University, Aramaki, Aoba-ku, Sendai, Miyagi 980-8578, Japan
[12] Research Center for Neutrino Science, Graduate School of Science, Tohoku University, Sendai 980-8578, Japan
[13] Leibnitz-Institut für Astrophysik Potsdam (AIP), An der Sternwarte 16, 14482 Potsdam, Germany
*Received 2011 September 5; accepted 2011 October 6; published 2011 December 22*

## ABSTRACT

In order to constrain the bolometric luminosities, dust properties, and molecular gas content of giant Lyα nebulae, the so-called Lyα blobs, we have carried out a study of dust continuum and CO line emission in two well-studied representatives of this population at $z \sim 3$: an Lyα blob discovered by its strong *Spitzer* Multiband Infrared Photometer 24 μm detection (LABd05) and the Steidel blob 1 (SSA22-LAB01). We find that the spectral energy distribution of LABd05 is well described by an active-galactic-nucleus–starburst composite template with $L_{\rm FIR} = (4.0 \pm 0.5) \times 10^{12}\ L_{\odot}$, comparable to high-$z$ submillimeter galaxies and ultraluminous infrared galaxies. New Large APEX Bolometer Camera 870 μm measurements rule out the reported Submillimeter Common-User Bolometer Array detection of the SSA22-LAB01 ($S_{850\,\mu{\rm m}} = 16.8$ mJy) at the $>4\sigma$ level. Consistent with this, ultradeep Plateau de Bure Interferometer observations with $\sim 2''$ spatial resolution also fail to detect any 1.2 mm continuum source down to $\approx$0.45 mJy beam$^{-1}$ ($3\sigma$). Combined with the existing (sub)millimeter observations in the literature, we conclude that the FIR luminosity of SSA22-LAB01 remains uncertain. No CO line is detected in either case down to integrated flux limits of $S_{\nu}\Delta V \lesssim 0.25$–$1.0$ Jy km s$^{-1}$, indicating a modest molecular gas reservoir, $M({\rm H_2}) < (1$–$3) \times 10^{10}\ M_{\odot}$. The non-detections exclude, with high significance ($12\sigma$), the previous tentative detection of a CO $J = 4$–3 line in the SSA22-LAB01. The increased sensitivity afforded by the Atacama Large Millimeter/submillimeter Array will be critical in studying molecular gas and dust in these interesting systems.

*Key words:* galaxies: formation – galaxies: high-redshift – intergalactic medium – radio lines: galaxies – submillimeter: galaxies

*Online-only material:* color figures

## 1. INTRODUCTION

Lyα nebulae (or Lyα "blobs") are extended sources at $z \sim$ 2–6 with typical sizes of the Lyα emission region of $\gtrsim 5''$ ($\gtrsim$50 kpc) and line luminosities of $L_{{\rm Ly}\alpha} \gtrsim 10^{43}$ erg s$^{-1}$, and are some of the most mysterious astronomical objects (e.g., Keel et al. 1999; Steidel et al. 2000; Francis et al. 2001; Matsuda et al. 2004, 2009, 2011; Dey et al. 2005; Saito et al. 2006; Smith & Jarvis 2007; Ouchi et al. 2009; Prescott et al. 2009; Prescott 2009; Yang et al. 2009, 2010). The nature of the extended Lyα emission is poorly understood. For example, Lyα blobs may represent galaxies forming via cold gas accretion (Fardal et al. 2001; Haiman et al. 2000; Dijkstra & Loeb 2009; Goerdt et al. 2010), galactic-scale outflows due to star formation (Taniguchi & Shioya 2000), or the result of intense radiative feedback from active galactic nuclei (AGNs; Haiman & Rees 2001; Geach et al. 2009).

To understand the nature of these Lyα blobs, we first need to constrain their energy budget, i.e., the bolometric luminosities of the galaxies within or in the vicinity of the Lyα halos and compare the available energy with the observed Lyα luminosities. Many Lyα blobs do not appear to contain bright UV continuum sources, bringing into question the nature of the underlying power source for these nebulae. Infrared (IR) and (sub)millimeter observations provide complementary information in such cases, by detecting and constraining the luminosity of any dust-enshrouded and obscured power sources (star forming or AGN) within the nebula. So far, a handful of Lyα blobs have been detected in the far-IR (FIR), suggesting that at least some Lyα blobs contain energy sources that can power the entire Lyα luminosity if only a few percent of their bolometric luminosities are converted to Lyα radiation (Chapman et al. 2004; Dey et al. 2005; Geach et al. 2005, 2009; Colbert et al. 2006, 2011). On the other hand, it appears that some Lyα blobs do not contain any obvious energy sources detectable at mid-IR or millimeter wavelengths (Nilsson et al. 2006; Smith et al. 2008); in these cases the Lyα emission has been attributed to gravitational cooling due to cold mode accretion (Kereš et al. 2005, 2009; Dekel et al. 2009).

[14] TABASGO Postdoctoral Fellow.

Despite the enormous star formation rates indicated by the FIR luminosities of some Ly$\alpha$ blobs (up to $\sim$1000 $M_\odot$ yr$^{-1}$), their molecular gas content—where the stars should form—has been mostly unconstrained. Therefore, it is important to understand whether there is enough cold molecular gas to power star formation in Ly$\alpha$ blobs or whether the molecular gas is depleted rapidly due to galactic-scale feedback either by superwind-driven shocks or photoionization by AGNs. In addition, if detected, carbon monoxide (CO) lines that trace the molecular gas can be used to probe the kinematics and the excitation conditions of the surrounding gas. Ly$\alpha$ blobs also present a unique opportunity to investigate the molecular gas content in environments that differ significantly from submillimeter galaxies (SMGs), high-redshift quasars (QSOs), or ultraluminous infrared galaxies (ULIRGs) that have been studied in the past (e.g., Solomon & Vanden Bout 2005). Most luminous Ly$\alpha$ blobs share the common property that they reside in overdense environments (Palunas et al. 2004; Matsuda et al. 2004; Prescott et al. 2008; Yang et al. 2009, 2010; Matsuda et al. 2009), suggesting that they may represent sites of massive galaxy formation. Furthermore, the discovery of spatially extended He II $\lambda$1640 emission and very weak metal emission lines from an Ly$\alpha$ blob at $z = 1.67$ suggests that the gas in the blob may be of low metallicity (Prescott et al. 2009).

In this paper, we present new (sub)millimeter observations of a $z = 2.656$ Ly$\alpha$ blob discovered by Dey et al. (2005) and measure its bolometric luminosity and dust properties. This blob (SST24 J1434110 +331733; hereafter LABd05) was discovered in the NOAO Deep and Wide Field Survey Boötes field (Jannuzi & Dey 1999) by its strong *Spitzer* Multiband Infrared Photometer (MIPS) 24 $\mu$m flux, indicating that as an IR-bright source it may be a ULIRG with a bolometric luminosity as large as (1–8) $\times$ $10^{13}$ $L_\odot$. While a 350 $\mu$m flux density of LABd05 had been measured as a part of a large Caltech Submillimeter Observatory (CSO) Submillimeter High Angular Resolution Camera (SHARC-II) program (Bussmann et al. 2009), the lack of (sub)millimeter observations covering both sides of the thermal dust peak of its spectral energy distribution (SED) prevented a direct constraint on its bolometric luminosity.

The best-studied Ly$\alpha$ blob (SSA22-LAB01 at $z = 3.09$) in the SSA22 protocluster region discovered by Steidel et al. (2000) has been reported to be associated with a bright SMG from Submillimeter Common-User Bolometer Array (SCUBA) observations (e.g., Chapman et al. 2004). However, follow-up observation with the Submillimeter Array (SMA) at higher spatial resolution ($\sim$2″) yielded a non-detection (Matsuda et al. 2007). Furthermore, an Atacama Submillimeter Telescope Experiment (ASTE) AzTEC single-dish observation with a beam size ($\approx$28″) larger than SCUBA (15″) also failed to detect this source down to $\sim$3 mJy (3$\sigma$) at 1.1 mm (Kohno et al. 2008; Tamura et al. 2009). Thus, the FIR luminosity of SSA22-LAB01 and the exact location of the dust continuum within the blob are uncertain. In this paper, we revisit SSA22-LAB01 with Large APEX Bolometer Camera (LABOCA) measurements whose wavelength and beam size are close to those of the previous SCUBA observations. We also present ultradeep millimeter interferometric continuum observations aiming to detect the possible compact sources within the blobs and, thus, to pinpoint the exact location of the energy source.

Prior to this work, the only blob targeted with CO observations was SSA22-LAB01. Chapman et al. (2004) reported a tentative detection of a CO(4–3) line, which implied a significant molecular gas reservoir, $M(\mathrm{H_2}) \sim 10^{11}$ $M_\odot$.[15] In this paper, we present a sensitive search for CO emission in this and the Ly$\alpha$ blob, LABd05. In Section 2, we describe our dust and CO observations. In Section 3.1, we present the SED of LABd05 and constrain its dust properties. In Section 3.2, we present the single-dish submillimeter observation to verify the previous FIR measurements, and the deep millimeter observation of SSA22-LAB01 conducted to determine the location of its submillimeter continuum emission. In Sections 3.3 and 3.4, we put constraints on the molecular gas contents of both Ly$\alpha$ blobs and compare their FIR and CO luminosities with those of other high-$z$ galaxies. In Section 4, we summarize the results. Throughout this paper, we adopt the following cosmological parameters: $H_0 = 70$ km s$^{-1}$ Mpc$^{-1}$, $\Omega_\mathrm{M} = 0.3$, and $\Omega_\Lambda = 0.7$.

## 2. OBSERVATIONS AND DATA ANALYSIS

### 2.1. Observations of LABd05

#### 2.1.1. IRAM-30 m 1.2 mm Observation

We observed LABd05 with the Max-Planck Millimeter Bolometer (MAMBO-2) on the Institut de Radio Astronomie Millimétrique (IRAM) 30 m telescope on 2005 May 18, 19, and 22. MAMBO-2 has a half-power spectral bandwidth from 210 to 290 GHz, with an effective band center of $\sim$250 GHz (1.20 mm) and a beam full width at half-maximum (FWHM) of 10.″7. LABd05 was observed in on–off observing mode under good weather conditions for $\sim$3 hr down to an rms of only 0.34 mJy (1$\sigma$) and was detected with a flux of 2.66 mJy (i.e., at 7.8$\sigma$).

#### 2.1.2. New Spitzer MIPS 70 $\mu$m and 160 $\mu$m Observations

Dey et al. (2005) reported non-detections of LABd05 at 70 $\mu$m and 160 $\mu$m based on the shallow observations of the Boötes field carried out with the MIPS instrument on board *Spitzer*. To further constrain the photometry of the source at these wavelengths, deeper pointed observations at 70 $\mu$m and 160 $\mu$m were obtained with the MIPS "photometry mode" as part of a General Observer program (ID 20303). The point-spread function sizes (FWHM) are 18″ and 40″ at 70 $\mu$m and 160 $\mu$m, respectively. We reduced these new observations with the MIPS Data Analysis Tool following the prescriptions described by Gordon et al. (2007), and derived fluxes for LABd05 using aperture photometry at the position of the object. However, no detection was obtained even in the deeper data. We estimated the 3$\sigma$ upper limits as the dispersion of fluxes measured in similar apertures randomly placed over the background of each image. Aperture corrections were applied following the MIPS Data Handbook of the Spitzer Science Center, which led to 3$\sigma$ limits of 9 mJy and 51 mJy at 70 $\mu$m and 160 $\mu$m, respectively.

#### 2.1.3. Archival Herschel SPIRE 250 $\mu$m and 350 $\mu$m data

The *Herschel* Spectral and Photometric Imaging Receiver (SPIRE) data were obtained in SPIRE/PACS parallel mode as part of the Herschel Multi-tiered Extragalactic Survey (HerMES) key project (PI: S. Oliver). Among the observations available for the Boötes field, a total of seven individual

[15] We converted the reported CO flux to the molecular gas mass using the same assumptions, cosmological parameters adopted in this paper (Section 3.3) and the CO(4–3)/CO(1–0) brightness ratio of $\simeq$0.5, i.e., the same as Chapman et al. (2004).

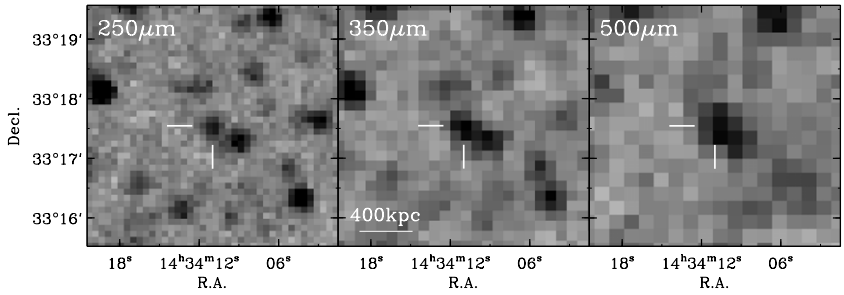


**Figure 1.** *Herschel*/SPIRE 250 $\mu$m, 350 $\mu$m, and 500 $\mu$m images of LABd05. The location of the MIPS 24 $\mu$m source is marked with the bars.

**Table 1**
Photometry of LABd05

| Facility | $\lambda_{obs}$ ($\mu$m) | $S_\nu$[a] (mJy) | Note |
|---|---|---|---|
| *Spitzer*/MIPS | 24 | $0.856 \pm 0.005$ | Dey et al. (2005) |
| | 70 | $< 9$ | This study |
| | 160 | $< 51$ | This study |
| CSO SHARC-II | 350 | $37 \pm 13$ | Bussmann et al. (2009) |
| *Herschel* SPIRE | 250 | $18.8 \pm 5.2$ | This study |
| | 350 | $26.9 \pm 5.1$ | This study |
| IRAM MAMBO-2 | 1200 | $2.76 \pm 0.35$ | This study |

**Note.** [a] $3\sigma$ upper limits if non-detection.

maps cover the source position. The data were processed in a standard fashion using Herschel Interactive Processing Environment (HIPE) 7.0 and the latest calibration files. While the seven observations were processed and calibrated individually, the resulting final map was created by combining all calibrated data and mapping all the scans simultaneously. We then used a SPIRE source extractor implemented in HIPE (based on Savage & Oliver 2007) to find unresolved sources and measure their fluxes using data for the approximate shape of the beam from the SPIRE Observers Manual (version 2.3). Photometric uncertainties were determined by measuring the pixel-to-pixel rms in an area of 180 arcmin$^2$ around the science target. This rms was determined in a cleaned map, which had all the sources detected in the previous step removed. We show the SPIRE 250, 350, and 500 $\mu$m images in Figure 1. The FWHMs of beam profiles are 18″, 25″, and 36″, respectively. In the 350 $\mu$m and 500 $\mu$m bands, the LABd05 is blended with the neighboring galaxy at the southwest direction. It was not possible to reliably obtain the 500 $\mu$m photometry due to severe blending. Our 350 $\mu$m SPIRE photometry ($27 \pm 5$ mJy) is consistent with the previous CSO)/SHARC-II observation ($S_{350\,\mu m} = 37 \pm 13$ mJy; Bussmann et al. 2009) within the uncertainties. We summarize the photometric observations in Table 1.

#### 2.1.4. IRAM-30m CO Observations

LABd05 was observed with the single pixel heterodyne receiver on the IRAM-30m telescope on UT 2005 May 18 and 21 in good weather conditions. We used the AB and CD receiver setups, with the AB receivers tuned to CO $J = 3$–2 (3 mm band, $\nu_{obs} = 94.614$ GHz) and the CD receivers tuned to CO $J = 5$–4 (2 mm band, $\nu_{obs} = 157.675$ GHz). The FWHM of the beam is 26″ and 16″, respectively. Average temperatures were 195 K at 2 mm and 135 K at 3 mm. Data were taken with a wobbler rate of 0.5 Hz and a wobbler throw of 50″ in azimuth. The pointing was checked frequently and was found to be stable within 3″ during the runs. Calibration was done every 12 minutes with standard hot/cold load absorbers, and we estimate fluxes to be accurate to within ∼10%–15% in both bands. We used the 512 × 1 MHz filter banks for the 3 mm receiver and the 256 × 4 MHz filter banks for the 2 mm receivers. As part of the data reduction, we dropped all scans with distorted baselines, subtracted linear baselines from the remaining spectra, and then rebinned to a velocity resolution of 40 km s$^{-1}$. The total on-source time is 3.4 hr for both CO observations. The conversion factors from K ($T_A^*$ scale) to Jy at our observed frequencies are 7.0 Jy K$^{-1}$ and 6.1 Jy K$^{-1}$ for the 2 mm and 3 mm bands, respectively. The resulting rms noises are 0.4 mK (2.8 mJy) and 0.45 mK (2.8 mJy) for 2 mm and 3 mm bands observations, respectively. We summarize the CO observations in Table 2.

### 2.2. Observations of SSA22-LAB01

#### 2.2.1. APEX LABOCA 870 $\mu$m Continuum Observations

The dust continuum of SSA22-LAB01 was observed at 870 $\mu$m using LABOCA (Siringo et al. 2009) at the Atacama Pathfinder Experiment (APEX) on 2011 August 18. Observations were carried out in the photometric on–off mode under good observing conditions (PWV = 0.5–0.7 mm). Throw and speed of the chopping secondary were set to 60″ and 1.5 Hz, respectively. Chopping was carried out in symmetric mode with a nodding time of 20 s. LABOCA's spatial resolution is 19.″2, comparable to the resolution of previous observations with SCUBA (Chapman et al. 2004). Calibration was achieved using Uranus (66.2 Jy at the time of observations) and the absolute calibration was estimated to be about 15%. Pointing was checked every 40 minutes on the nearby QSO J2225−045 and found to be stable within 3.″6 (rms). The data were reduced using the BoA software package. The total integration time on SSA22-LAB01 is 2 hr 20 minutes (on+off, including instrumental overheads). Our observations yield a non-detection of the source with $S_{870\,\mu m} = -2.9 \pm 2.7\ (\pm 4.0)$ mJy beam$^{-1}$. The first error is the rms calculated from error propagation via the rms on the reduced bolometer time line. The second error in parentheses is the uncertainty calculated from the dispersion of the individual scans, and therefore represents a more conservative error estimate.

#### 2.2.2. PdBI 1.2 mm Continuum Observations

We observed SSA22-LAB01 between 2010 May and 2011 January with the Plateau de Bure Interferometer (PdBI) in D configuration (Project ID: T0B2). The on-source observing time, corresponding to the full array of six antennae, was 5.9 hr. We set the phase center at the reported SCUBA submillimeter galaxy (SMM J221725.97+001238.9). The 1 mm receiver WideX was tuned at 241.5 GHz, corresponding to 1.25 mm in the

**Table 2**
CO Line Observations for LABd05 and SSA22-LAB01

| Source | $z_{Ly\alpha}$[a] | Transition | $\nu_{obs}$ (GHz) | $\sigma_{rms}$ (mJy) | $\delta v$[b] (km s$^{-1}$) | $L'_{CO}$ ($J$+1→$J$)[c] ($10^{10}$ K km s$^{-1}$ pc$^2$) | $M(H_2)$[d] ($10^{10}$ $M_\odot$) |
|---|---|---|---|---|---|---|---|
| LABd05 | 2.656 ± 0.006 | 3–2 | 94.614 | 2.8 | 42.0 | < 3.90 | < 3.12 |
| | | 5–4 | 157.675 | 2.8 | 42.0 | < 1.37 | ... |
| SSA22-LAB01 | 3.102 ± 0.005 | 3–2 | 84.299 | 0.53 | 100 | < 1.47 | < 1.17 |
| | | 4–3 | 112.300 | 2.0 | 26.7 | < 1.64 | ... |

**Notes.**
[a] Redshifts determined from Ly$\alpha$ lines (Dey et al. 2005; Bower et al. 2004).
[b] Channel bandwidth.
[c] 3$\sigma$ upper limits assuming CO line width $\Delta V = 400$ km s$^{-1}$.
[d] 3$\sigma$ upper limits assuming $X_{CO} = 0.8\ M_\odot$ (K km s$^{-1}$ pc$^2$)$^{-1}$ and constant brightness temperatures.

observed and ∼400 $\mu$m in the rest frame. The total bandwidth of our dual polarization mode observations was 3.6 GHz. The data were calibrated through observations of standard bandpass (3C 454.3, 2223−052), phase/amplitude (2131−021, 2145+067, 2223−052), and flux calibrators (MWC 349), and reduced with the GILDAS software packages[16] CLIC and MAPPING. The final map, created using natural weighting, has an rms noise of 0.15 mJy integrated over the full bandwidth. Note that this new observation is approximately four times deeper than the previous SMA observations ($\sigma_{rms}$ = 1.4 mJy at 880 $\mu$m; Matsuda et al. 2007) and one of the deepest observations ever carried out at ∼1 mm on a single target. The FWHM of the beam is 2.″4 × 1.″6 (18 kpc × 12 kpc) at 1.25 mm (P.A. = 14.°9), similar to that of the SMA observations (2.″4 × 1.″9).

### 2.2.3. PdBI CO Observations

Observations for SSA22-LAB01 were carried out using the PdBI in 2002 May–June (112 GHz, tuned on the CO $J$ = 4–3 line at $z$ = 3.1; Project ID: M021) and in 2010 June–July (84 GHz, tuned on the CO $J$ = 3–2 line; Project ID: U045). Data were collected in compact D configuration, with baselines ranging between 24 and 113 m. Phase calibrators were observed every 20 minutes. The rms phase errors are ∼20°. The primary amplitude calibrators were 3C454.3 (variable, at ∼25 Jy at 3 mm during our observations), MWC 349 (not variable, ∼1 Jy), and 2223–052 (∼3.5 Jy, also used as phase calibrator). Data at 112 GHz (84 GHz) were collected using the narrow band (WideX) receiver. System temperatures ranged between 120 and 250 K. Typical uncertainties in the flux scales and overall calibration are about 10%. The data processing program used water vapor monitoring receivers at 22 GHz on each antenna to correct amplitudes and phases for short-term changes in atmospheric water vapor. We weighted visibilities according to the inverse square of the system temperature, and natural weights were applied when creating the maps, in order to boost the sensitivity. The primary beam size of PdBI is 56″ (42″) at 84 GHz (112 GHz). No cleaning was applied. In the case of WideX observation with a large bandwidth, we also place an upper limit on the continuum ($\sigma_{rms}$ = 0.15 mJy (3$\sigma$). We summarize the CO observations in Table 2.

## 3. RESULTS

### 3.1. Spectral Energy Distribution of LABd05

Using our new FIR photometry from *Spitzer* MIPS, *Herschel* SPIRE, and MAMBO–2, we compare the SED of LABd05 with those of starbursts and AGNs in order to measure the bolometric luminosity and investigate whether we can discriminate possible energy sources of the blob.

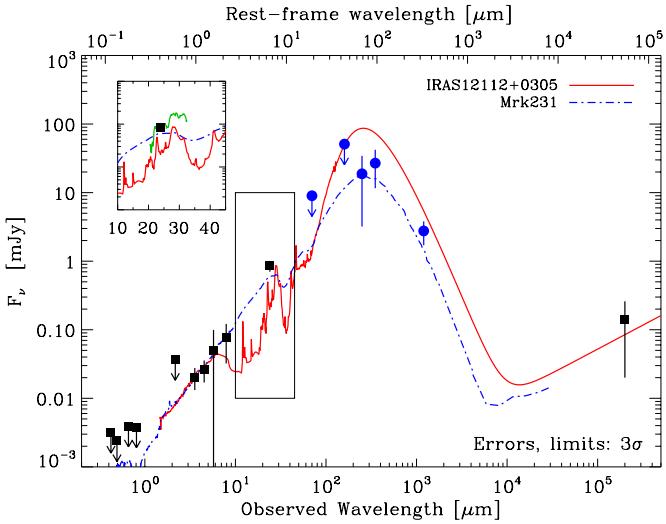


**Figure 2.** Spectral energy distribution of LABd05 from the rest-frame UV to radio. The squares represent the photometry compiled by Dey et al. (2005) and the large circles are the *Spitzer* MIPS 70 $\mu$m, 160 $\mu$m, *Herschel* SPIRE 250 $\mu$m, 350 $\mu$m, and IRAM-30m/MAMBO-2 1.2 mm photometry from this work. The error bars and upper limits are given at 3$\sigma$. The solid and dot-dashed lines represent the SED templates of IRAS12112+0305 (starburst dominated; Rieke et al. 2009) and Mrk 231 (AGN dominated; Polletta et al. 2007). Templates are scaled to match the 3.6 $\mu$m, 4.5 $\mu$m, and 5.8 $\mu$m flux densities. The inset shows the IRS spectrum from Colbert et al. (2011). The AGN template shows good agreement with data while the starburst template (IRAS12112+0305) overestimates the FIR flux by a factor of ∼5.
(A color version of this figure is available in the online journal.)

Figure 2 shows the SED of LABd05 from optical to radio wavelength in the observed frame. The squares and large circles represent the flux measurements from Dey et al. (2005) and new constraints from this study, respectively. We also show the *Spitzer* Infrared Spectrograph (IRS) spectrum ($\lambda_{obs}$ = 19.5–38 $\mu$m) from Colbert et al. (2011), which reveals that strong polycyclic aromatic hydrocarbon (PAH) features contribute ∼50% of MIPS 24 $\mu$m flux. For comparison, we show the SED templates of IRAS12112+0305 and the Seyfert 1 galaxy Mrk 231 that are redshifted to $z$ = 2.66 and scaled to match the Infrared Array Camera (IRAC) 3.6 $\mu$m, 4.5 $\mu$m, and 5.8 $\mu$m flux densities (rest frame 1–1.5 $\mu$m). IRAS12112+0305 and Mrk 231 represent local analogs whose IR SEDs are dominated by star formation and AGNs, respectively. We select IRAS12112+0305 as a representative template from

[16] http://www.iram.fr/IRAMFR/GILDAS

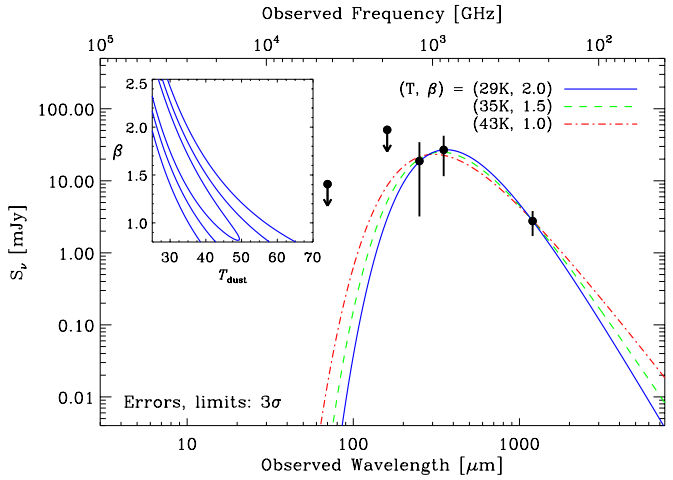


**Figure 3.** Spectral energy distribution of LABd05 focusing on mid-IR to millimeter wavelengths. New data points from this work are fitted with a modified blackbody SED with a dust temperature $T_d$ and an emissivity index $\beta$. The error bars and upper limits are given at $3\sigma$. The left inset shows the likelihood distribution of the fits in $T_d$ and $\beta$ space. The contours represent the $1\sigma$, $2\sigma$, and $3\sigma$ confidence intervals. We find a dust temperature $T_d$ of 44, 35, and 29 K for different $\beta = 1$, 1.5, and 2, respectively. While there is a degeneracy between $T_d$ and $\beta$, we find that the model with colder dust temperature ($T_d \sim$ 30 K) provides a better fit to the data.

(A color version of this figure is available in the online journal.)

11 LIRG/ULIRG templates compiled by Rieke et al. (2009) by searching for a template that best matches our data. The Mrk 231 template is also selected by searching for the best-fit templates from the AGN-dominated templates compiled by Polletta et al. (2007).

We find that the AGN template (Mrk 231) is able to fit the full SED of LABd05 from the rest frame 1 $\mu$m to 350 $\mu$m reasonably well, but additional PAH emission is required to reproduce the strong 7.7 $\mu$m features in the observed *Spitzer* IRS spectrum, and the Mrk 231 template slightly underpredicts the long-wavelength FIR flux densities. On the other hand, the starburst template overestimates the FIR luminosity by a factor of $\approx$5 and fails to fit the IRAC 8.0 $\mu$m and MIPS 24 $\mu$m data points as discussed by Dey et al. (2005). Clearly, more sophisticated SED modeling is required and observations around the rest frame 2–10 $\mu$m are essential for fully constraining the SED.

Since our new (sub)millimeter observations cover both sides of the thermal dust peak, we can constrain the dust temperature and the FIR luminosity of LABd05. We fit the data with a modified blackbody SED (Hildebrand 1983) with the following functional form at $h\nu/kT_d \lesssim 1$:

$$S_\nu \propto \frac{\nu^{(3+\beta)}}{\exp(h\nu/kT_d) - 1}, \quad (1)$$

where $T_d$ is the effective dust temperature and $\beta$ is the dust emissivity index with $1 \lesssim \beta \lesssim 2$. In Figure 3, we show the best-fit models and the likelihood distribution of $T_d$ and $\beta$ parameters. While $T_d$ and $\beta$ are degenerate, we find that the model with the higher $\beta$ and lower dust temperature $T_d$ shows better agreement with the data. Insufficient data on the shorter wavelength side of the peak prevents us from constraining the lower/upper limits on $T_d/\beta$, so we choose $\beta = 2$ as a nominal value and determine the best fit dust temperature $T_d = 29^{+2}_{-1}$ K. For reference, we also show the fits for fixed $\beta = 1$ and 1.5 which results in $T_d \simeq 44^{+4}_{-3}$ and $35^{+2}_{-2}$ K, respectively.

Using these SED fits, we derive the far-IR and bolometric luminosity ($L_{\rm FIR}$ and $L_{\rm bol}$) of LABd05. We find $L_{\rm FIR}$(40–1000 $\mu$m) = $(4.0 \pm 0.52) \times 10^{12}\ L_\odot$ and $L_{\rm bol} = (8.6 \pm 1.1) \times 10^{12}\ L_\odot$, consistent with SMGs and ULIRGs. To obtain the bolometric luminosity, we apply the $L_{\rm bol} \approx 2.15\ L_{\rm FIR}$ correction based on the Mrk 231 SED template. Note that the SPIRE 350 $\mu$m flux density, $\nu L_\nu = (3.5 \pm 0.6) \times 10^{12}\ L_\odot$, alone can roughly constrain the $L_{\rm FIR}$ since the SPIRE band corresponds to the peak of the SED. We estimate the dust mass, $M_d$, using

$$M_{\rm dust} = \frac{1}{1+z} \frac{S_\nu D_L^2}{\kappa_\nu^{\rm rest} B(\nu_{\rm rest}, T_d)}, \quad (2)$$

where $S_\nu$ is the observed flux density, $D_L$ is the luminosity distance, $\kappa_\nu^{\rm rest}$ is the rest-frame dust mass absorption coefficient, and $B(\nu, T_d)$ is the Plank function at the rest frame. We adopt $T_d = 29$ K and $\beta = 2$ from our best-fit model and $\kappa_{125\mu m} = 26.4$ cm$^2$ g$^{-1}$ (Dunne et al. 2003), which corresponds to $\kappa_{850\mu m} = 0.57$ cm$^2$ g$^{-1}$ assuming $\kappa \propto \nu^\beta$. We find a total dust mass of $M_{\rm dust} = (1.4 \pm 0.7) \times 10^9\ M_\odot$. Note that this dust mass estimate strongly depends on the choice of $\kappa_\nu^{\rm rest}$ and $T_d$. The absorption coefficient $\kappa_{850\,\mu\rm m}$ is uncertain to a factor of $\sim$2, e.g., $\kappa_{850\,\mu\rm m} = 0.77$ cm$^2$ g$^{-1}$ (Dunne et al. 2000, 2011) or $\kappa_{850\,\mu\rm m} = 0.38$ cm$^2$ g$^{-1}$ (Milky Way dust model; Draine 2003). Or if we adopt the lower temperature $T_d = 35$ K for $\beta = 1.5$, the dust mass will decrease by a factor of 2.2.

### 3.2. Non-detection of Continuum Emission in SSA22-LAB01

SSA22-LAB01 was not detected down to $S_{870\,\mu\rm m} = 8.1$–12 mJy beam$^{-1}$ ($3\sigma$) with new APEX/LABOCA single-dish observations that have a similar beam size (19″) to the previous SCUBA 850 $\mu$m observations (15″). Chapman et al. (2004) reported that SSA22-LAB01 contains a bright submillimeter galaxy: SMM J221725.97+001238.9 with the flux densities of $S_{850\,\mu\rm m} = 16.8 \pm 2.9$ mJy and $S_{450\,\mu\rm m} = 45.1 \pm 15.1$ mJy, respectively.[17] If we assume simple model SEDs with $(T_d, \beta) =$ (40 K, 2) and (30 K, 1.5), we expect an 870 $\mu$m flux density of $S_{870\,\mu\rm m} = 15.7$ – 16.1 mJy, which would be detected by LABOCA with $4\sigma$–$6\sigma$ significance depending on the LABOCA error estimates (Section 2.2.1). This non-detection is consistent with essentially all measurements of the source in the literature, in particular the SMA observations by Matsuda et al. (2007). In that study, SSA22-LAB01 was also not detected down to $S_{880\,\mu\rm m} = 4.2$ mJy beam$^{-1}$ ($3\sigma$) with a $\sim$2″ spatial resolution. They proposed, as explanation, that the dust emission (reported by SCUBA) is extended on spatial scales larger than 4″ such that the interferometer observation would resolve out this smooth component. However, the original SCUBA observation is not verified by our LABOCA observation for which this argument does not hold. Furthermore, an ASTE-AzTEC single-dish observation with a larger beam size (FWHM $\approx$ 28″) than SCUBA (15″) also failed to detect dust continuum down to $\sim$3 mJy ($3\sigma$) at 1.1 mm (Kohno et al. 2008; Tamura et al. 2009), thus contradicting the SCUBA measurement at the $4.5\sigma$ confidence level. In Figure 4, we show the upper limits derived from our LABOCA and PdBI observations with the existing (sub)millimeter observations of the SSA22-LAB01. These observations are summarized in Table 3. The solid and dot-dashed

[17] Slightly different values for the SCUBA 850 $\mu$m and 450 $\mu$m fluxes are reported in Chapman et al. (2001, 2004, 2005). Since all the flux measurements agree with each other within uncertainties, we adopt the values reported by Chapman et al. (2004) throughout the paper.

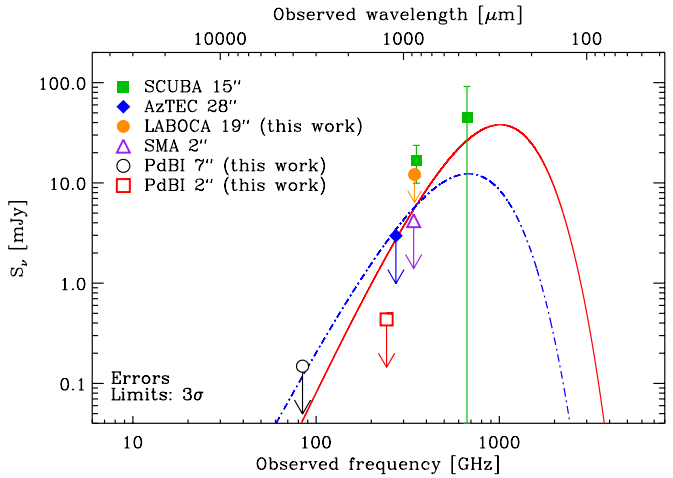


**Figure 4.** FIR flux densities of SSA22-LAB01. Different symbols represent the (sub)millimeter observations with different instruments and beams sizes (see Table 3). The filled and open symbols indicate the flux measurements from single dish and interferometer observations, respectively. All the uncertainties and upper limits are in $3\sigma$ level. For illustration purposes, the solid and dot-dashed lines represent the modified blackbody SEDs normalized at the $S_{850\,\mu m} = 6$ mJy with $(T_d, \beta) = (40\ \mathrm{K}, 2)$ and $(30\ \mathrm{K}, 1.5)$, respectively. The upper limits from all other instruments disagree with the SCUBA 850 $\mu$m measurement.

(A color version of this figure is available in the online journal.)

lines represent the two model SEDs normalized at $S_{850\,\mu m} = 6$ mJy, showing the possible range of the extrapolated flux densities at various wavelengths. The upper limits from all other (sub)millimeter observations (both single-dish and interferometer) are inconsistent with the SCUBA measurements. Therefore, we conclude that the previous SCUBA measurements are not reliable.

Given that SSA22-LAB01 contains multiple galaxies and that the total star formation rate within the blob is at least $\sim$220 $M_\odot$ yr$^{-1}$ (Matsuda et al. 2007), it is critical to identify galaxies by their dust emission within the Ly$\alpha$ halo which produce most of the bolometric luminosity. In order to detect dust emission from individual galaxies within SSA22-LAB01, we compare our deep PdBI 1.2 mm continuum map with the locations of the UV and *Spitzer* IRAC sources identified by Chapman et al. (2004) and Geach et al. (2007). In Figure 5, we show the PdBI 1.2 mm continuum map of SSA22-LAB01 and overlay the contours of this map on the Ly$\alpha$ and *BV* broadband images (Matsuda et al. 2004). The pointing center of the LABOCA observation is marked with a large cross (positional uncertainty of 3.″6) and a dashed circle gives the beam size of 19″. This pointing center is the same as the phase center of the PdBI observations. We show locations of the *Spitzer*/IRAC sources marked as LAB 1 *abcde* (Geach et al. 2007) in Figure 5. Out of these five IRAC sources, three sources (LAB 1 *a*, *b*, and *e*) are likely associated with the SSA22-LAB01 (Geach et al. 2007; Uchimoto et al. 2008). We find that no significant emission is detected from these three galaxies while there is a $\sim 4\sigma$ peak (R.A. $= 22^h17^m26^s.06$, decl. $= 00°12'35''.1$) between LAB 1*a* and 1*b*. Furthermore, none of the $\sim 3\sigma$ peaks within the field of view of our 1.2 mm map agree with other UV sources in the field (right panel in Figure 5). Therefore, we conclude that none of the known optical or near-IR emitting galaxies within the SSA22-LAB01 Ly$\alpha$ halo are detected at 1.2 mm down to 0.45 mJy beam$^{-1}$ ($3\sigma$). Future observations with the Atacama Large Millimeter/submillimeter Array (ALMA) will be required to verify this tentative $\sim 4\sigma$ peak.

**Table 3**
FIR Observations of SSA22-LAB01

| Facility | Wavelength ($\mu$m) | Beam Size (arcsec) | $S_\nu$[a] (mJy) | Reference[b] |
|---|---|---|---|---|
| SCUBA | 850 | 15 | $16.8 \pm 2.9$ | (1) |
| | 450 | 8 | $45.1 \pm 15.1$ | |
| AzTEC | 1100 | 28 | <3.0 | (2) |
| SMA | 880 | $2.5 \times 1.9$ | <4.2 | (3) |
| LABOCA | 870 | 19 | <12.0 | This study |
| PdBI | 1250 | $2.4 \times 1.6$ | <0.45 | This study |
| PdBI | 3500 | $8.4 \times 5.4$ | <0.15 | This study |

**Notes.**
[a] $3\sigma$ upper limits if non-detection.
[b] (1) Chapman et al. 2001, 2004, 2005; (2) Kohno et al. 2008; Tamura et al. 2009; (3) Matsuda et al. 2007.

Without any formal detection at (sub)millimeter wavelengths, the FIR luminosity of SSA22-LAB01 remains highly uncertain. We place upper limits on the FIR luminosity of SSA22-LAB01 using simple model SEDs to provide the possible range of $L_{\rm FIR}$. If we normalize the SEDs at the 870 $\mu$m $3\sigma$ upper limit, we obtain $L_{\rm FIR} < 3.1 \times 10^{12}\ L_\odot$ and $1.2 \times 10^{13}\ L_\odot$ depending on the choice of the model SED, $(T_d, \beta) = (30\ \mathrm{K}, 1.5)$ and $(40\ \mathrm{K}, 2)$, respectively. If we adopt our 1.2 mm PdBI measurement, the individual galaxies within the blob have $L_{\rm FIR} < (0.39\text{–}2.1) \times 10^{12}\ L_\odot$ ($3\sigma$).

In addition to the PdBI 1.2 mm continuum observation, we also place an upper limit on the 3 mm flux density using the PdBI CO observation (see Section 3.3). No continuum source is detected in the integrated channel map over 4 GHz bandwidth, resulting in $3\sigma$ limit of 0.15 mJy beam$^{-1}$ with a beam size of 8.″4 × 5.″4.

### 3.3. Molecular Gas Content of LABd05 and SSA22-LAB01

In Figure 6, we show the spectra of the CO lines for the LABd05 and the SSA22-LAB01 obtained from the IRAM-30m and PdBI, respectively. For LABd05, we show the spectra for the CO $J = 3$–2 and CO $J = 5$–4 lines with a velocity resolution of $\delta v = 40$ km s$^{-1}$. For SSA22-LAB01, we show the CO $J = 3$–2 and CO $J = 4$–3 transition with $\delta v = 100$ km s$^{-1}$ and 27 km s$^{-1}$, respectively. The rms noise per channel ranges from 0.5 to 2.8 mJy beam$^{-1}$ (Table 2) depending on the instruments and the transitions.

Because of the width of spectral the bandwidth ($\sim$2000 km s$^{-1}$), knowing the accurate redshift is critical in this CO detection experiment. In Figure 6, we show the velocity range of CO lines that corresponds to the range spanned by Ly$\alpha$: $z = 2.656 \pm 0.006$ for LABd05 (Dey et al. 2005) and $z = 3.102 \pm 0.005$ for SSA22-LAB01 (Bower et al. 2004; Matsuda et al. 2005). Given that Ly$\alpha$ emission lines from star-forming galaxies at $z = 2$–3 could be redshifted against the optically thin nebular lines (i.e., systemic velocity) by 250–1000 km s$^{-1}$ (e.g., Pettini et al. 2001; Steidel et al. 2004, 2010) due to either galactic-scale outflows or absorption by the intervening intergalactic medium, we note that CO lines, which are also expected to emit near the systemic velocity (e.g., Greve et al. 2005), could be located blueward (higher $\nu_{\rm obs}$) of the horizontal bars. For LABd05, we also show the velocity range corresponding to the optically thin He II $\lambda$1640 emission that originates from the central region of the Ly$\alpha$ nebula. At least for LABd05, these two estimates for CO line centers are in good agreement, therefore we conclude

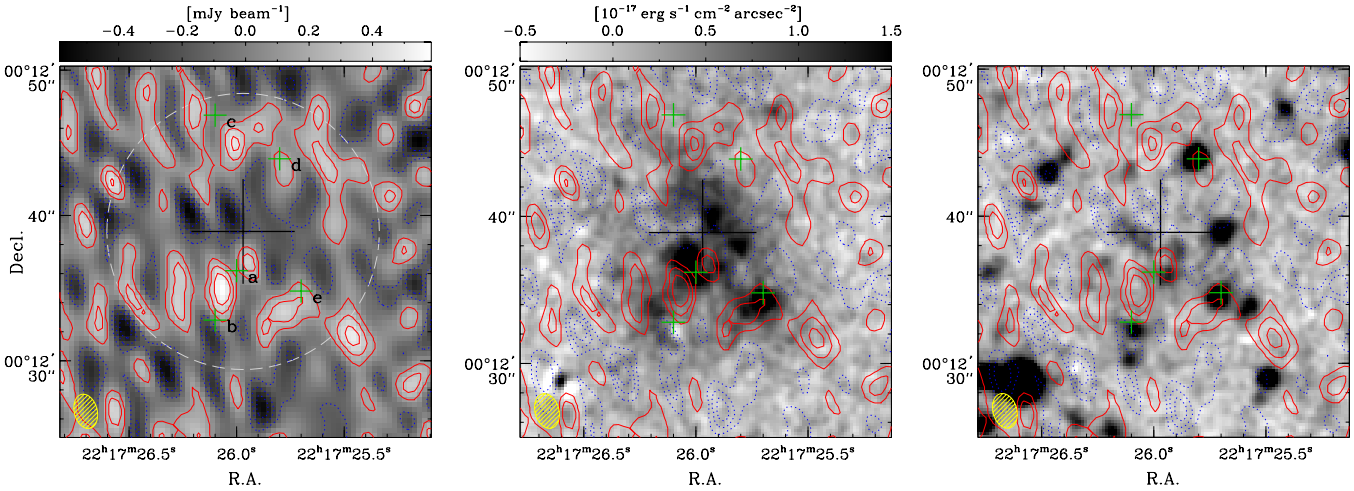


**Figure 5.** Left: PdBI 1.2 mm continuum map of SSA22-LAB01. The synthesized beam has an FWHM of 2.″4 × 1.″6 (P.A. = 14.°9). The phase center of the PdBI is marked with a large cross—its size indicates the positional uncertainty of the LABOCA pointing. The LABOCA beam (FWHM = 19″) is represented by the dashed circle. The small crosses represent the locations of the *Spitzer* IRAC sources (Geach et al. 2007). No significant continuum source is detected above 3$\sigma$ level at the location of these galaxies. Middle and right: PdBI 1.2 mm continuum contours superimposed on the Subaru/Suprime-Cam Ly$\alpha$ and *BV* broadband images (Matsuda et al. 2004), respectively. The contours show $-3\sigma$, $-2\sigma$, $-1\sigma$, $1\sigma$, $2\sigma$, and $3\sigma$ with $\sigma = 0.15$ mJy beam$^{-1}$.

(A color version of this figure is available in the online journal.)

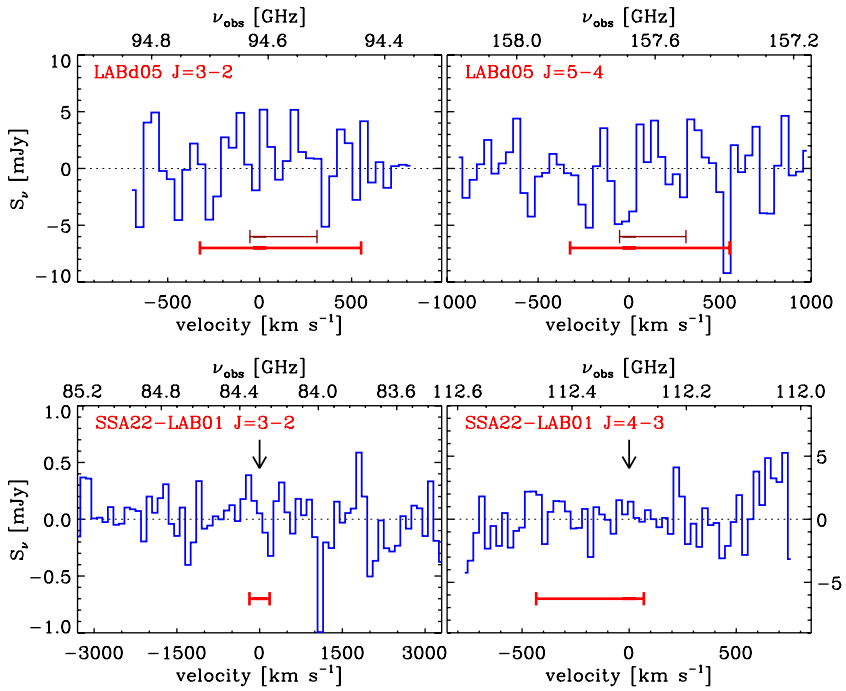


**Figure 6.** Top: IRAM-30m CO spectra for CO $J = 3$–2 and CO $J = 5$–4 transitions for LABd05. Both spectra have velocity resolutions of $\delta v = 40$ km s$^{-1}$. The thick and thin horizontal bars represent the expected velocity range estimated from the Ly$\alpha$ and He II emission line in the optical (Dey et al. 2005). Bottom: PdBI CO spectra for CO $J = 3$–2 and CO $J = 4$–3 transitions of SSA22-LAB01 with $\delta v = 100$ km s$^{-1}$ and 27 km s$^{-1}$, respectively. Note that the scales of the *y*-axis are different between the two panels. The thick horizontal bars represent the expected velocity range estimated from the Ly$\alpha$ line (Bower et al. 2004). The vertical arrows indicate the location of the previous tentative CO detection (Chapman et al. 2004). No CO line is detected in either case.

(A color version of this figure is available in the online journal.)

that it is unlikely that any potential CO line would fall outside of the spectral bandwidth covered by our IRAM-30m observations. We note that, for SSA22-LAB01, the CO $J = 4$–3 spectra obtained with the old narrowband receivers at PdBI were taken with a limited bandwidth and no other optically thin emission lines were available to double check the systemic redshift. On the other hand, the PdBI CO $J = 3$–2 spectrum obtained with the new WideX correlator has a very wide spectral coverage (4 GHz; 14000 km s$^{-1}$), enough to cover any plausible velocity offsets between Ly$\alpha$ and CO lines. We conclude that no significant CO emission is detected above the rms noise near the expected velocities in both systems.

In the case of SSA22-LAB01, we also inspect whether any tentative source can be detected in the integrated channel maps. In Figure 7, we show the channel maps summed over $\Delta V = 1000$ km s$^{-1}$ intervals centered at $-1500$, $-500$, 500, 1500 km s$^{-1}$ from the Ly$\alpha$ velocity center. While there could be a possible 3$\sigma$ detection near the phase center in the

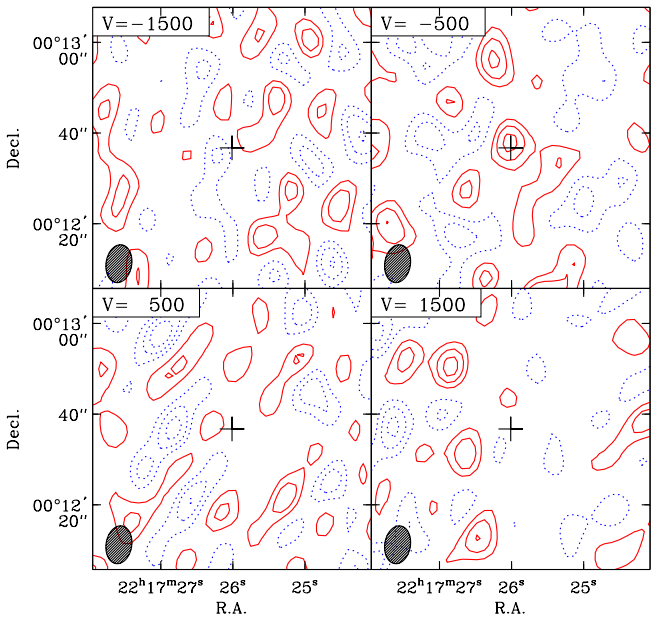


**Figure 7.** Integrated channel map of the CO $J = 3$–2 line for SSA22-LAB01. Each channel map is integrated over a 1000 km s$^{-1}$ bandwidth centered at the velocities shown in the upper left corners. The contours are at $-3\sigma_{\rm rms}$, $-2\sigma_{\rm rms}$, $-1\sigma_{\rm rms}$, $1\sigma_{\rm rms}$, $2\sigma_{\rm rms}$, and $3\sigma_{\rm rms}$, where $\sigma_{\rm rms}$ is the rms noise per 1000 km s$^{-1}$ velocity width (0.172 mJy beam$^{-1}$). The phase center is marked with a cross in each panel. While there is a possible $3\sigma$ detection near the phase center at the $v = -500$ km s$^{-1}$ channel, no significant CO line is detected at above $3\sigma$ level per 100 km s$^{-1}$ channel in that bin.

(A color version of this figure is available in the online journal.)

$v = -500$ km s$^{-1}$ channel map (upper right panel of Figure 7), this marginal detection in the integrated map corresponds to only $\sim 1.7\sigma$ signal per 100 km s$^{-1}$ channels. Because we are not able to extract a reliable spectrum from this tentative source, we conclude that no significant CO line is detected above the 3 × rms noise near the expected velocities. More sensitive observations using ALMA will test whether or not this tentative emission is real.

Our new PdBI observation for SSA22-LAB01 rules out the previous tentative CO detection at high significance. Chapman et al. (2004) reported a tentative ($3.2\sigma$) detection of a CO $J = 4$–3 line from SSA22-LAB01 using the Owens Valley Radio Observatory Millimeter Array. The reported intensity is $S_\nu \sim 10$ mJy at the peak with a line width of ∼400 km s$^{-1}$. In Figure 6, we indicate the location of earlier tentative CO detection with arrows. As described in detail below, our $3\sigma$ limit for the integrated CO $J = 4$–3 flux from PdBI is $S_\nu \Delta V < 0.62$ Jy km s$^{-1}$, i.e., we exclude the previous detection at high significance ($12\sigma$).

Using these non-detections, we put constraints on CO line luminosities and molecular gas mass of the blobs. Following Solomon & Vanden Bout (2005), the CO luminosity $L'_{\rm CO}$ (in K km s$^{-1}$ pc$^2$) is given by

$$L'_{\rm CO} = 3.25 \times 10^7 \, S_{\rm CO} \, \Delta V \, \nu_{\rm obs}^{-2} \, D_L^2 \, (1+z)^{-3} \ , \qquad (3)$$

where $\nu_{\rm obs}$ is the observing frequency (in GHz) and $D_L$ is the luminosity distance (in Mpc) to the source at a redshift $z$. For our non-detection, we adopt a $3\sigma$ upper limit on the velocity-integrated flux $S_{\rm CO}\Delta V \equiv 3(\Delta V/\delta v)^{1/2} \, (\delta v \, \sigma_{\rm rms})$ in Jy km s$^{-1}$, where $\Delta V$ is the CO line width, $\delta v$ is the channel bandwidth, and $\sigma_{\rm rms}$ is the rms noise value per channel, respectively. As the CO line width is unknown, we adopt $\Delta V = 400$ km s$^{-1}$, consistent with FWHM = 300–450 km s$^{-1}$ measured from the optically thin H$\alpha$ lines in two other Ly$\alpha$ blobs in the Extended Chandra Deep Field South (Yang et al. 2011). For LABd05, we obtain $3\sigma$ CO line luminosity limits, $L'_{\rm CO(5-4)} < 1.37 \times 10^{10} \, (\Delta V/400)^{1/2}$ K km s$^{-1}$ pc$^2$ and $L'_{\rm CO(3-2)} < 3.90 \times 10^{10} \, (\Delta V/400)^{1/2}$ K km s$^{-1}$ pc$^2$. In the case of the SSA22-LAB01, we obtain the upper limits of $L'_{\rm CO(4-3)} < 1.6 \times 10^{10} \, (\Delta V/400)^{1/2}$ and $L'_{\rm CO(3-2)} < 1.5 \times 10^{10} \, (\Delta V/400)^{1/2}$ K km s$^{-1}$ pc$^2$.

The upper limits for the total molecular gas mass, $M(\rm H_2)$, can be derived using a CO-to-$\rm H_2$ conversion factor between CO $J = 1$–0 luminosity and molecular gas mass, $X_{\rm CO}$. Here we adopt $X_{\rm CO} \approx 0.8 \, M_\odot$ (K km s$^{-1}$ pc$^2$)$^{-1}$, which was proposed as appropriate for starburst environments found in ULIRGs (Downes & Solomon 1998). If we assume a constant brightness temperature for the different CO transitions, i.e., CO $J = 1$–0 luminosity as defined by Equation (3) is the same as those of upper $(J+1) \rightarrow J$ transitions, the upper limits on the molecular gas mass can be given as $M(\rm H_2) < 3.1$ and $1.2 \times 10^{10} \, M_\odot \, (\Delta V/400)^{1/2} (X_{\rm CO}/0.8)$ for LABd05 and SSA22-LAB01, respectively. Note that, for submillimeter galaxies and QSOs in a similar redshift range, the gas has been found to be thermalized at least up to the $J = 3$–2 transition as the ratio $L'_{\rm CO(3-2)}/L'_{\rm CO(1-0)}$ is close to unity (≈0.8, e.g., Weiss et al. 2007). Therefore, we use only the $J = 3$–2 transition to estimate limits on $L'_{\rm CO(1-0)}$ and $M(\rm H_2)$. We note that our final $M(\rm H_2)$ estimates are strongly dependent not only on the intrinsic excitation but also on the choice of $X_{\rm CO}$. For example, if we adopted $X_{\rm CO} \approx 4.5 \, M_\odot$ (K km s$^{-1}$ pc$^2$)$^{-1}$, the Milky Way value, the resulting molecular gas mass limits would increase by a factor of ∼5.

### 3.4. $L_{FIR}$–$L'_{\rm CO}$ Correlation

With the FIR luminosity and the upper limit on CO luminosity in hand, we investigate whether $L'_{\rm CO}$ and $L_{\rm FIR}$ of the LABd05 are consistent with the known $L_{\rm FIR}$–$L'_{\rm CO}$ scaling relations. For SSA22-LAB01, the ratio between $L_{\rm FIR}$ and $L'_{\rm CO}$ remains unconstrained so far. For nearby starburst and spiral galaxies with $L_{\rm FIR} \lesssim 10^{12} \, L_\odot$, the correlation has the form $\log L_{\rm FIR} = (1.26 \pm 0.08) \times \log L'_{\rm CO} - 0.81$ (Gao & Solomon 2004). When ULIRGs, SMGs, radio galaxies (RGs), and QSOs are included, the relation becomes slightly steeper, $\log L_{\rm FIR} = (1.39 \pm 0.05) \times \log L'_{\rm CO} - 1.76$, but still holds over five orders of magnitude in $L_{\rm FIR}$ (Riechers et al. 2006). For LABd05 with $L_{\rm FIR} = (4.0 \pm 0.5) \times 10^{12} \, L_\odot$, we expect $L'_{\rm CO} = (2.2 \pm 1.9) \times 10^{10}$ K km s$^{-1}$ pc$^2$ for the ULIRG/SMG/RG/QSO relation. Therefore, we find that our $3\sigma$ upper limit on $L'_{\rm CO}$ for LABd05 is consistent with the known $L_{\rm FIR}$–$L'_{\rm CO}$ scaling relations. In terms of the continuum-to-line luminosity ratio, we find that $L_{\rm FIR}/L'_{\rm CO} > 100$, which is consistent with the $L_{\rm FIR}/L'_{\rm CO} = 125 - 240 \, L_\odot$ (K km s$^{-1}$ pc$^2$)$^{-1}$ for the galaxies with $L_{\rm FIR} \sim 10^{12-13} \, L_\odot$. Note that due to the nonlinear relation between $L_{\rm FIR}$ and $L'_{\rm CO}$, the ratio $L_{\rm FIR}/L'_{\rm CO}$ has a large spread depending on $L_{\rm FIR}$.

## 4. SUMMARY AND CONCLUDING REMARKS

We have obtained IR and (sub)millimeter observations of the two best-studied Ly$\alpha$ blobs, LABd05 and SSA22-LAB01, in order to constrain their energy budgets (i.e., the bolometric luminosity) and dust properties. We find that LABd05 has a high FIR luminosity, $L_{\rm FIR} = 4.0 \times 10^{12} \, L_\odot$, comparable to values found for high-$z$ SMGs and ULIRGs. The NIR-to-FIR SED of LABd05 is well described by the AGN–starburst composite template (Mrk 231). For SSA22-LAB01, no 870 $\mu$m

continuum is detected down to 8.1–12 mJy beam$^{-1}$ ($3\sigma$) in the LABOCA single-dish observation contrary to the originally reported SCUBA measurement. To detect the dust emission from individual galaxies within SSA22-LAB01, we obtained a very deep 1.2 mm observation of SSA22-LAB01. No 1.2 mm continuum is detected down to $\approx$0.45 mJy beam$^{-1}$ ($3\sigma$) at $\sim 2''$ resolution. Combined with the existing extensive (sub)millimeter observations from the literature, we conclude that the previously published SCUBA detection (Chapman et al. 2004) is not reliable. We place $3\sigma$ upper limits of $L_{\rm FIR} < (3.1\text{–}12) \times 10^{12}\,L_{\odot}$ for the total FIR luminosity of the blob and $L_{\rm FIR} < (0.39\text{–}2.1) \times 10^{12}\,L_{\odot}$ for the individual galaxies within the blob.

To investigate the molecular gas content in Ly$\alpha$ blobs, we carried out a sensitive search for CO lines in the two Ly$\alpha$ blobs. No CO line is detected down to an integrated flux limit of $S_{\nu}\Delta V \lesssim 0.25\text{–}1.0$ Jy km s$^{-1}$ constraining the molecular mass to be less than $M(\rm H_2) \approx (1\text{–}3) \times 10^{10}\,M_{\odot}$ ($3\sigma$ limit), assuming a constant brightness temperature and a CO-to-$\rm H_2$ conversion factor for the starburst galaxies. The non-detections from our new search exclude the previous tentative ($\sim 3\sigma$) detection of the CO $J = 4\text{–}3$ line toward SSA22-LAB01 reported by Chapman et al. (2004) with a high significance ($12\sigma$). We find that the FIR-to-CO luminosity ratio of $L_{\rm FIR}/L'_{\rm CO} \gtrsim 100\,L_{\odot}\,(\rm K\,km\,s^{-1}\,pc^2)^{-1}$ for LABd05 is consistent with the scaling relations of ULIRG/SMG/QSO/RG. While our sensitive CO searches already place interesting limits on the brightest Ly$\alpha$ blobs, future observations with ALMA will allow us to routinely detect CO in similar systems (0.1 Jy km s$^{-1}$ for $\sim$1 hr integration) beyond the sensitivity limits that are accessible today.

We thank the anonymous referee for the prompt report and the helpful comments. We thank Jan Martin Winters and Melanie Krips for supporting our PdBI CO and 1.2 mm observations. Y.Y. thanks Elisabete Da Cunha and Brent Groves for the helpful discussions on the SED fitting. The research activities of A.D. are supported by the National Optical Astronomy Observatory, which is operated by the Association of Universities for Research in Astronomy (AURA) under cooperative agreement with the National Science Foundation. Based on observations carried out with the IRAM Plateau de Bure Interferometer and the IRAM-30m Telescope. IRAM is supported by INSU/CNRS (France), MPG (Germany), and IGN (Spain). This publication is based on data acquired with the Atacama Pathfinder Experiment (APEX). APEX is a collaboration between the Max-Planck-Institut für Radioastronomie, the European Southern Observatory, and the Onsala Space Observatory. This work is based in part on observations made with the *Spitzer Space Telescope*, which is operated by the Jet Propulsion Laboratory, California Institute of Technology under a contract with NASA. *Herschel* is an ESA space observatory with science instruments provided by European-led Principal Investigator consortia and with important participation from NASA.

*Facilities:* IRAM:Interferometer, *Spitzer* (MIPS), APEX (LABOCA), IRAM:30m (MAMBO-2), Herschel (SPIRE)

## REFERENCES

Bower, R. G., Morris, S. L., Bacon, R., et al. 2004, MNRAS, 351, 63
Bussmann, R. S., Dey, A., Borys, C., et al. 2009, ApJ, 705, 184
Chapman, S. C., Blain, A. W., Smail, I., & Ivison, R. J. 2005, ApJ, 622, 772
Chapman, S. C., Lewis, G. F., Scott, D., et al. 2001, ApJ, 548, L17
Chapman, S. C., Scott, D., Windhorst, R. A., et al. 2004, ApJ, 606, 85
Colbert, J. W., Scarlata, C., Teplitz, H., et al. 2011, ApJ, 728, 59
Colbert, J. W., Teplitz, H., Francis, P., et al. 2006, ApJ, 637, L89
Dekel, A., Birnboim, Y., Engel, G., et al. 2009, Nature, 457, 451
Dey, A., Bian, C., Soifer, B. T., et al. 2005, ApJ, 629, 654
Dijkstra, M., & Loeb, A. 2009, MNRAS, 400, 1109
Downes, D., & Solomon, P. M. 1998, ApJ, 507, 615
Draine, B. T. 2003, ARA&A, 41, 241
Dunne, L., Eales, S., Edmunds, M., et al. 2000, MNRAS, 315, 115
Dunne, L., Eales, S. A., & Edmunds, M. G. 2003, MNRAS, 341, 589
Dunne, L., Gomez, H. L., da Cunha, E., et al. 2011, MNRAS, 417, 1510
Fardal, M. A., Katz, N., Gardner, J. P., et al. 2001, ApJ, 562, 605
Francis, P. J., Williger, G. M., Collins, N. R., et al. 2001, ApJ, 554, 1001
Gao, Y., & Solomon, P. M. 2004, ApJ, 606, 271
Geach, J. E., Alexander, D. M., Lehmer, B. D., et al. 2009, ApJ, 700, 1
Geach, J. E., Matsuda, Y., Smail, I., et al. 2005, MNRAS, 363, 1398
Geach, J. E., Smail, I., Chapman, S. C., et al. 2007, ApJ, 655, L9
Goerdt, T., Dekel, A., Sternberg, A., et al. 2010, MNRAS, 407, 613
Gordon, K. D., Engelbracht, C. W., Fadda, D., et al. 2007, PASP, 119, 1019
Greve, T. R., Bertoldi, F., Smail, I., et al. 2005, MNRAS, 359, 1165
Haiman, Z., & Rees, M. J. 2001, ApJ, 556, 87
Haiman, Z., Spaans, M., & Quataert, E. 2000, ApJ, 537, L5
Hildebrand, R. H. 1983, QJRAS, 24, 267
Jannuzi, B. T., & Dey, A. 1999, in ASP Conf. Ser. 191, Photometric Redshifts and the Detection of High Redshift Galaxies, ed. R. Weymann et al. (San Francisco, CA: ASP), 111
Keel, W. C., Cohen, S. H., Windhorst, R. A., & Waddington, I. 1999, AJ, 118, 2547
Kereš, D., Katz, N., Fardal, M., Davé, R., & Weinberg, D. H. 2009, MNRAS, 395, 160
Kereš, D., Katz, N., Weinberg, D. H., & Davé, R. 2005, MNRAS, 363, 2
Kohno, K., Tamura, Y., Hatsukade, B., et al. 2008, in ASP Conf. Ser. 399, Panoramic Views of Galaxy Formation and Evolution, ed. T. Kodama, T. Yamada, & K. Aoki (San Francisco, CA: ASP), 264
Matsuda, Y., Iono, D., Ohta, K., et al. 2007, ApJ, 667, 667
Matsuda, Y., Nakamura, Y., Morimoto, N., et al. 2009, MNRAS, 400, L66
Matsuda, Y., Yamada, T., Hayashino, T., et al. 2004, AJ, 128, 569
Matsuda, Y., Yamada, T., Hayashino, T., et al. 2005, ApJ, 634, L125
Matsuda, Y., Yamada, T., Hayashino, T., et al. 2011, MNRAS, 410, L13
Nilsson, K. K., Fynbo, J. P. U., Møller, P., Sommer-Larsen, J., & Ledoux, C. 2006, A&A, 452, L23
Ouchi, M., Ono, Y., Egami, E., et al. 2009, ApJ, 696, 1164
Palunas, P., Teplitz, H. I., Francis, P. J., Williger, G. M., & Woodgate, B. E. 2004, ApJ, 602, 545
Pettini, M., Shapley, A. E., Steidel, C. C., et al. 2001, ApJ, 554, 981
Polletta, M., Tajer, M., Maraschi, L., et al. 2007, ApJ, 663, 81
Prescott, M. K. M. 2009, PhD thesis, Univ. Arizona
Prescott, M. K. M., Dey, A., & Jannuzi, B. T. 2009, ApJ, 702, 554
Prescott, M. K. M., Kashikawa, N., Dey, A., & Matsuda, Y. 2008, ApJ, 678, L77
Riechers, D. A., Walter, F., Carilli, C. L., et al. 2006, ApJ, 650, 604
Rieke, G. H., Alonso-Herrero, A., Weiner, B. J., et al. 2009, ApJ, 692, 556
Saito, T., Shimasaku, K., Okamura, S., et al. 2006, ApJ, 648, 54
Savage, R. S., & Oliver, S. 2007, ApJ, 661, 1339
Siringo, G., Kreysa, E., Kovács, A., et al. 2009, A&A, 497, 945
Smith, D. J. B., & Jarvis, M. J. 2007, MNRAS, 378, L49
Smith, D. J. B., Jarvis, M. J., Lacy, M., & Martínez-Sansigre, A. 2008, MNRAS, 389, 799
Solomon, P. M., & Vanden Bout, P. A. 2005, ARA&A, 43, 677
Steidel, C. C., Adelberger, K. L., Shapley, A. E., et al. 2000, ApJ, 532, 170
Steidel, C. C., Shapley, A. E., Pettini, M., et al. 2004, ApJ, 604, 534
Steidel, C. C., Erb, D. K., Shapley, A. E., et al. 2010, ApJ, 717, 289
Tamura, Y., Kohno, K., Nakanishi, K., et al. 2009, Nature, 459, 61
Taniguchi, Y., & Shioya, Y. 2000, ApJ, 532, L13
Uchimoto, Y. K., Suzuki, R., Tokoku, C., et al. 2008, PASJ, 60, 683
Weiss, A., Downes, D., Walter, F., & Henkel, C. 2007, in ASP Conf. Ser. 375, From Z-Machines to ALMA: (Sub)Millimeter Spectroscopy of Galaxies, ed. A. J. Baker et al. (San Francisco, CA: ASP), 25
Yang, Y., Zabludoff, A., Eisenstein, D., & Davé, R. 2010, ApJ, 719, 1654
Yang, Y., Zabludoff, A., Jahnke, K., et al. 2011, ApJ, 735, 87
Yang, Y., Zabludoff, A., Tremonti, C., Eisenstein, D., & Davé, R. 2009, ApJ, 693, 1579